NJP354812 on 27 August 2010

New Journal of Physics
The open-access journal for physics

Manipulation of quantum state transfer in cold Rydberg atom collisions

J S Cabral[1], J M Kondo[1], L F Gonçalves[1], L G Marcassa[1], D Booth[2], J Tallant[2] and J P Shaffer[2]

[1] Instituto de Física de São Carlos, Universidade de São Paulo, Caixa Postal 369, 13560-970 São Carlos-SP, Brazil
[2] Homer L Dodge Department of Physics and Astronomy, The University of Oklahoma, 440 W Brooks Street, Norman, OK 73019, USA
E-mail: xxx

New Journal of Physics **12** (2010) 000000 (15pp)
Received 19 April 2010
Published xxx
Online at http://www.njp.org/
doi:10.1088/1367-2630/12/9/000000

Abstract. We investigate the role of the dc Stark effect in multilevel pairwise interactions between cold Rydberg atoms. We have observed the decay of $nD+nD$ quasi-molecules by detecting the products in the $(n+2)P$ state after pulsed excitation for $29 \leqslant n \leqslant 41$. The decay rate can be manipulated with a dc electric field and requires a consideration of the multilevel nature of the process to explain the observations. The time dependence of the $(n+2)P$ signal is found to support a time-dependent picture of the dynamics.

Q1

Contents

1. Introduction

There has been increasing interest in ultracold Rydberg atoms over the last several years. The primary reason for this attention is that interactions between Rydberg atoms are strong and lead to many interesting and useful phenomena. For example, the interactions between Rydberg atoms can be strong enough to block the laser excitation of more than one Rydberg excitation in a volume determined by the Rydberg atom interaction strength and laser energy bandwidth. The interaction between Rydberg atoms detunes the collective two (or more) excitation states from resonance with the exciting laser. This effect is called Rydberg atom dipole blockade and can be used to coherently create a collective state, as the single Rydberg excitation in the blockaded volume is a coherent superposition of a Rydberg excitation of each atom in the volume. Efforts to develop Rydberg atom quantum gates hinge on the Rydberg atom dipole blockade effect [1, 2]. Recent experiments on Rydberg atom dipole blockade with two atoms have shown that this type of collective excitation is possible [3, 4]. As a second example, the starting point for investigating many-body phenomena with ultracold Rydberg gases is also the Rydberg atom pair interactions [5]. The presence and degree of many-body interactions in a cold Rydberg gas can, in principle, be controlled by state selection, choice of density and application of external fields, so these systems are promising for exploring the onset of many-body phenomena. Finally, the generation of exotic Rydberg molecules during the last year has generated excitement [6, 7]. Some of these molecules are bound by Rydberg atom interactions and have bond lengths of several microns! The bonds between the Rydberg atoms that form these molecules can be controlled by the application of an external electric field. Knowledge of Rydberg atom interactions and how they can be manipulated can be seen, from these examples, to be of central importance to this field, and considerable effort has been made to experimentally investigate them [7]–[12].

To date, often only one or two pairwise atomic potentials, considering only dipole–dipole interaction while ignoring dc electric fields, have been used to interpret cold Rydberg atom experiments. Even if a few pair states and their respective sub-states are considered, this situation is surprising, because the Rydberg atom energy level spacing has an n^{-3} dependence on principal quantum number, n. In many cases, there are a large number, >10, of pair potential curves that are energetically close to each other. These pair potentials can form a complex system of multi-state potential energy curve crossings [13]. The potential energy curve crossings between these interacting pair states lead to nonadiabatic processes. In addition, the electric fields that are present in most experiments can cause significant changes to the field-free Rydberg atom pair potentials. The electric fields can significantly alter the dynamics by modifying the structure of the curve crossings. Unless only the longest range part of the potentials where curve crossings are not present play an important role in a particular experiment, it appears extremely difficult to tune the interactions between Rydberg atoms so that only a single pair of pair potentials needs to be considered. It is possible, and likely, that a large number of states play an important role in many experiments, even when many-body effects are not significant. Consequently, it is imperative to understand the interplay of multiple interaction potentials and how they are influenced by electric fields.

In this work, we investigate how nonadiabatic multichannel decay of Rydberg atom diatomic quasi-molecules is affected by dc electric fields. Specifically, we study the decay of $nD + nD$ Rydberg pair states through the observation of $(n+2)P$ atomic products 100 ns after their excitation in an Rb magneto-optical trap (MOT). The experimentally observed $(n+2)P$

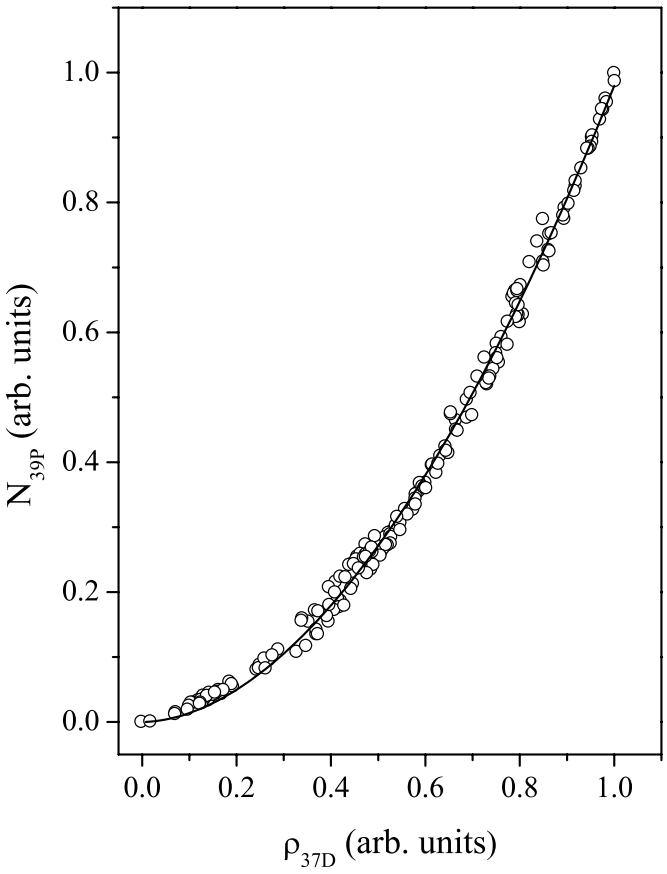

Figure 1. $39P$ population (N_{39P}) as a function of ρ_{37D}. The data were normalized to its maximum signal along both the axes. The symbols are the experimental data and the line is a power-law fit to the $37D$ density, ρ_{37D}^{δ}, where δ is a fitting parameter. The fit gives $\delta = 1.9 \pm 0.1$.

population is quadratically dependent on the nD atomic density, ρ_{nD}, for $29 \leqslant n \leqslant 41$. This confirms that the process involves two nD atoms so the experiment probes the pair interactions between these states, as shown in figure 1. Figure 1 shows the $39P$ population, N_{39P}, as a function of ρ_{37D}. The data were normalized to its maximum signal along both the axes. The full line is a power-law fit to the $37D$ density, ρ_{37D}^{δ}, where δ is a fitting parameter. The fit shows that the N_{39P} is proportional to $\rho_{37D}^{1.9\pm0.1}$.

Consideration of the dc Stark effect, multipole interaction and atomic fine structure is required to explain the experimental data. The dynamics that lead to the production of $(n+2)P$ atoms are complex because the $nD+nD$ pair potential curves have many avoided crossings that cause nonadiabatic transitions. At short range, where many curves cross, there is a complicated structure and quadrupolar interactions are important. The short range structure of the interaction potentials can be contrasted to the structure at long range where the interactions are dominated by dipole–dipole interactions. We find that the decay of $nD+nD$ pairs results in population transfer into $(n+2)P+(n-2)l$ pairs (where $l \geqslant F$) and that the decay rate for this process can be significantly influenced by a dc electric field. We also compare the initial time evolution of the $(n+2)P$ products to the transition rates between the relevant states and find that the theory agrees well with the experimental data, suggesting that the experiment can be interpreted

dynamically as a system undergoing a nonadiabatic transition [15]. Our experiment is not sensitive to the anisotropic interactions that take place between Rydberg atoms in electric fields because the experiment averages over all impact parameters in the MOT. Anisotropic effects for some of the Rydberg states used in this work have been studied in [14]. Our results are consistent with the prior work [14], but seek to provide additional insight into the short-ranged nonadiabatic processes that lead to atomic state changes.

2. Experimental setup

The experimental setup has been described in a recent paper [12]. Under typical conditions 2.5×10^6 Rydberg atoms are excited in an Rb MOT at a peak $\rho_{nD} \sim 5 \times 10^9\,\mathrm{cm}^{-3}$. The Rydberg excitation is provided by a pulsed laser beam at 480 nm, which has a bandwidth of $0.05\,\mathrm{cm}^{-1}$ and a peak irradiance of $\sim 780\,\mathrm{MW\,cm}^{-2}$. The background electric field is estimated to be $< 80\,\mathrm{mV\,cm}^{-1}$ and the external applied dc electric field, ϵ, is controlled with a resolution of $30\,\mathrm{mV\,cm}^{-1}$. The Rydberg atoms and their quantum states are detected by collecting the electrons produced by pulsed electric field ionization (PFI) with a channel electron multiplier. Two boxcar gates are used to selectively detect the nD and $(n+2)P$ signals. In the experiments, the delays between optical excitation and PFI were varied from 100 ns to 8 μs. As an example, we show the time-resolved electron signal for $37D$ and $39P$ in figure 2 at $\epsilon = 2\,\mathrm{V\,cm}^{-1}$. The size of the $39P$ electron signal detected 100 ns after the $37D + 37D$ state excitation is $\sim 10\%$ of the $37D$ atomic signal. This signal is larger by a factor of 3–10 than that found for a case where ac Stark shifts lead to population transfer [12].

We used data like that presented in figures 1 and 2 taken for the other n to calculate a two-body rate constant, K, as a function of n for several ϵ. Since K is defined by $\mathrm{d}N_{(n+2)P}/\mathrm{d}t = K \int \rho_{nD}^2\,\mathrm{d}V$, where V is the laser excitation volume, we can obtain K using the experimental density and laser interaction volume. Figure 3 shows the theoretical and experimental K as a function of n for $\epsilon = 0.5$ and $2.0\,\mathrm{V\,cm}^{-1}$ at a PFI delay time of 100 ns. Note that there is approximately a factor of 3–4 difference between the rates for some n at the two ϵ used in the experiment.

3. Calculations

To explain the results shown in figure 3, we calculated the interactions between atom pairs around the $nD + nD$ asymptote as a function of internuclear distance, R. The calculation includes dipole–dipole, dipole–quadrupole and quadrupole–quadrupole interactions as well as the dc Stark effect and atomic fine structure [9, 10]. Figures 4(a) and (b) show the $37D + 37D$ potential curves and surrounding states for $M = 0$, where M is the projection of the angular momentum on the internuclear axis, at $\epsilon = 2\,\mathrm{V}$ and $0.5\,\mathrm{V\,cm}^{-1}$, respectively, as examples. The states in figures 4(a) and (b) are labeled by the asymptotic atomic pair states to which each potential correlates. The calculations indicate that the avoided crossings are predominantly due to a dipole–dipole interaction but that quadrupolar interactions cannot be neglected. For example, the dipole–quadrupole interaction is less than 5% of the dipole–dipole interaction at $R \sim 2\,\mu\mathrm{m}$ for $\epsilon = 0.5\,\mathrm{V\,cm}^{-1}$. The quadrupole–quadrupole interaction is less than 0.01% of the dipole–dipole interaction for the $37D + 37D$ pair states at the same R. At short range, $R < 1.5\,\mu\mathrm{m}$ for $37D + 37D$, the picture is more complex. In this range, the

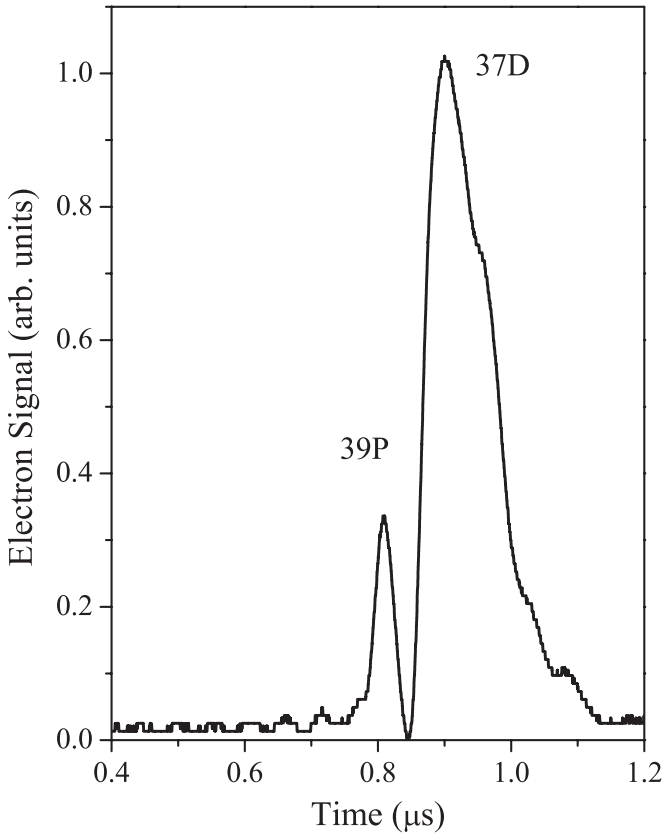

Figure 2. Time-resolved electron signal for $37D$ and $39P$ at $\epsilon = 2\,\mathrm{V\,cm^{-1}}$. The population transfer from $37D$ to $39P$ is about 10%.

quadrupole interactions can be critical as shown in figure 5. Figure 5(a) shows a calculation for $37D + 37D$ with quadrupole interactions, while figure 5(b) shows the calculation without quadrupole interactions. In figure 5(b), a potential curve crossing that leads to significant population transfer to $39P$ has disappeared because there is no quadrupolar interactions. This particular example demonstrates that the short-ranged crossings can have a dramatic dependence on the quadrupole interactions.

Since these calculations take place in an electric field, all of the interaction potentials have some angular dependence. However, these effects are small when compared to the van der Waals interactions that are most important for interpreting our experiments. Aside from the mixing of m_j atomic states caused by the field, there is further mixing from the many other states via dipolar and quadrupolar interactions. The angular contributions to each potential from each of these sources tend to average away in our computations. Presumably, these effects suppress the angular dependence that is found when a particular pair state is brought into Forster resonance with another pair state [14]. It is also true that we did not observe any angular dependence in the experiment. In addition to the weak angular dependence found in the calculations, the yield is experimentally averaged over all impact parameters in the trap. It is on these experimental and computational grounds that we ignore the angular dependence in the Rydberg atom interaction potentials in the interpretation of the experiments in this paper. These assumptions should be the subject of further experiments. Q2

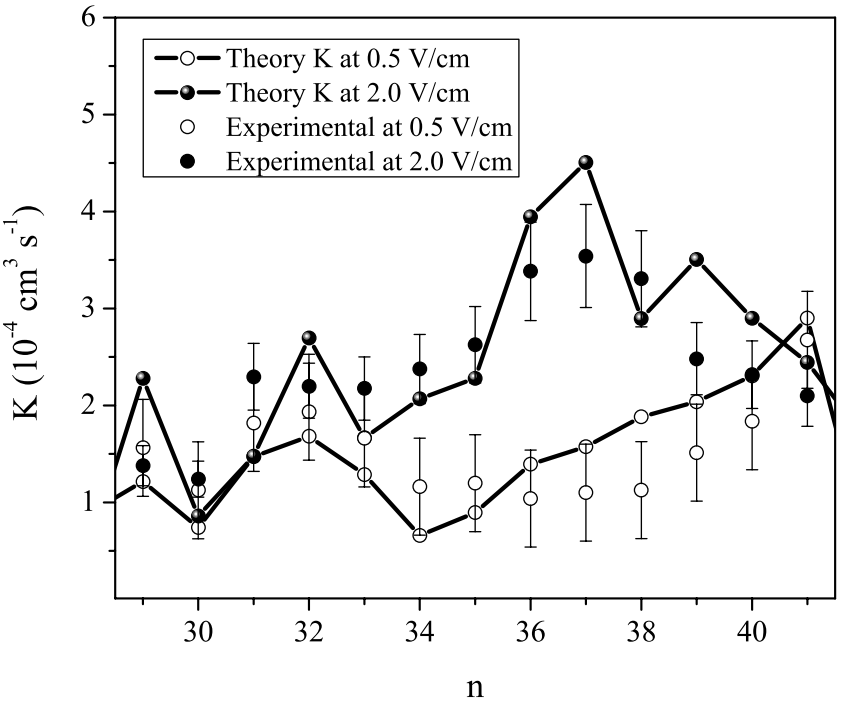

Figure 3. Theoretical and experimental K for 0.5 and 2.0 V cm^{-1} as a function of n for a PFI delay time of 100 ns.

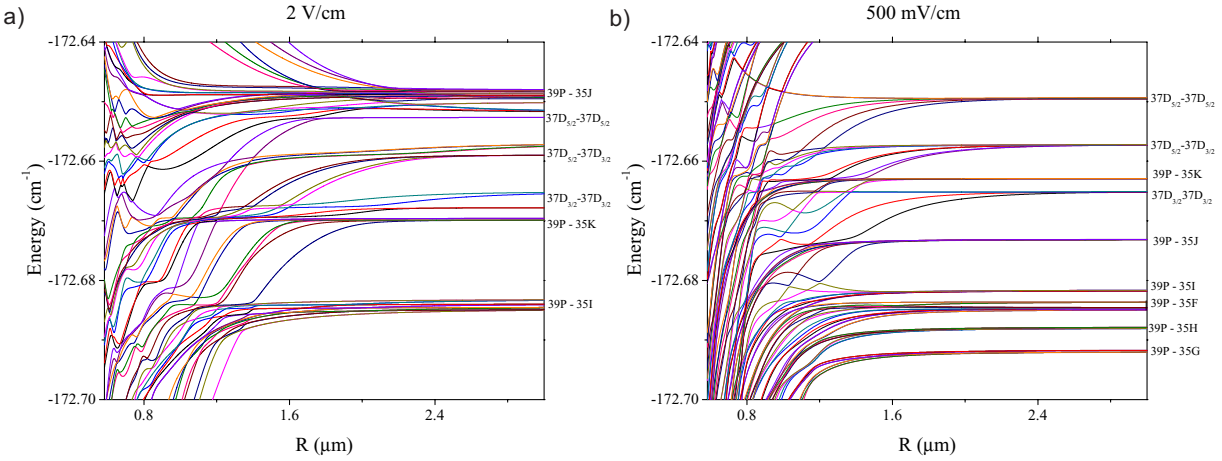

Figure 4. $37D + 37D$ and surrounding potential energy curves for $M = 0$ at (a) $\epsilon = 2$ V cm^{-1} and (b) $\epsilon = 0.5$ V cm^{-1}.

The probability of an event resulting in transfer of population from the $nD + nD$ pair state to the $(n+2)P$ atomic state can be calculated semiclassically using the Landau–Zener approximation. We do not expect the population transfer to $(n+2)P$ to result from free atom collisions because the Rydberg atoms are approximately frozen on the timescale of the short PFI delay times. An Rb atom at the Doppler temperature moves 10 nm in 100 ns. On the timescale of the 100 ns PFI delay, blackbody radiation does not play a role. For an 8 μs PFI delay, the

blackbody decay can be extracted from the signal that results from the molecular decay, as described later.

The pair potentials exhibit many avoided crossings between different pair states. At R where the crossings are, the system can make a nonadiabatic transition and change state. The avoided crossings occur at R that vary with n. For example, at $n = 29$, $R = 1.3\,\mu$m at the outermost crossing, whereas at $n = 41$, $R = 1.7\,\mu$m at the outermost crossing. The crossings for the $nD + nD$ states were found using a computer search algorithm that locates the R where an avoided crossing occurs between two calculated potential curves. The algorithm was later checked by carefully going through the plotted potentials visually and computationally by increasing the number of neighboring pair potentials that were compared. There are some pair states that are separated in energy such that many other pair states lie energetically between two sets of interacting pairs. These avoided crossings are difficult to detect with the algorithm.

We calculated the nonadiabatic transition probability for each crossing using the semi-classical Landau–Zener formula. The velocity used in the Landau–Zener formula is approximated by calculating the kinetic energy of the system at the crossing point by assuming that the excitation occurred near the dissociation limit. This assumption is made for simplicity and is consistent with approximating the excitation to have taken place where the Franck–Condon factors and the probability of finding a near neighbor are largest, near the outer turning point, near the dissociation limit where the electronic character is almost pure $nD + nD$. We also assume that the system makes a single transition attempt within the Landau–Zener picture because the inner turning points of the $nD + nD$ potentials are at very short range and many of the curves cross states of higher electronic orbital angular momentum that are not coupled to $(n + 2)P$ states and the PFI delay times are relatively short. At short range, it is probable, from an analysis of the potential curves, that Penning ionization and other decay mechanisms lead to different product states.

If the atoms are assumed to be stationary, consistent with the 100 ns and 8 μs PFI delay times chosen so that no free excited Rydberg atoms collide, then a state changing event can only take place if an $nD + nD$ quasi-molecule is initially excited. Therefore, there must be a pair of atoms with a nearest-neighbor distance between the inner wall, $R_{\min}$, of the pair potential and an outer separation distance, $R_{\max}$, which defines molecular excitation. We take the outer separation distance to be the point where the potential is as deep as the average kinetic energy of the atoms in the MOT. $R_{\min}$ for each potential is chosen by finding the inner turning point of that potential at the dissociation limit. The entire calculation of the rate is rather insensitive to $R_{\min}$ because the atomic density is low enough in the experiments that the probability to find a pair of atoms with internuclear separation near $R_{\min}$ is essentially 0. $R_{\max}$ is chosen to be the largest internuclear separation where it would be expected that the two atoms would attract each other or in other words form a molecule. The value of $R_{\max}$ determined by this criterion is found for each potential. Although $R_{\min}$ and $R_{\max}$ parameterize the model, they are not arbitrary and we justify them on a reasonable physical basis. For $n = 29$ at $\epsilon = 0.5\,\mathrm{V\,cm^{-1}}$, $R = 0.5\,\mu$m at the inner point and 2.2 μm at the outer point. Similarly, for $n = 41$ at $\epsilon = 0.5\,\mathrm{V\,cm^{-1}}$, $R = 0.9\,\mu$m at the inner point and 3.3 μm at the outer point. The probability of finding a nearest-neighbor atom within the range of R given by these criteria is

$$P_{nn} = \int_{R_{\min}}^{R_{\max}} 4\pi\rho R^2\, \mathrm{e}^{-4\pi R^3\rho/3}\, \mathrm{d}R, \tag{1}$$

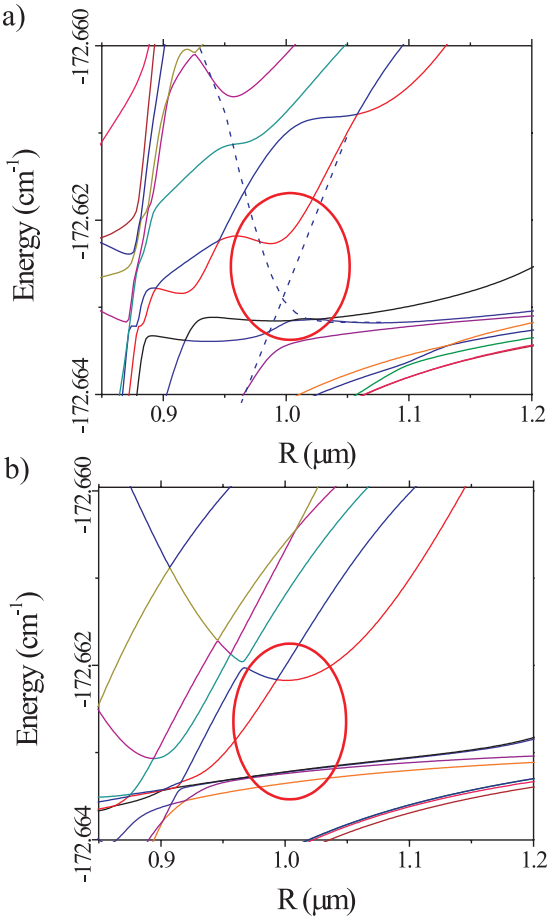

Figure 5. Theoretical potential energy curves. (a) Potential energy curves calculated with quadrupolar and dipolar interactions. (b) Potential energy curves calculated with only dipole interactions. The electric field is $\epsilon = 0.5\,\mathrm{V\,cm^{-1}}$ for both calculations. The crossing at $R \sim 1.0\,\mu$m is not present unless the quadrupolar interactions are included in the calculation.

where ρ is the ground state atom density [16]. For the densities used in the experiment $\sim 80\%$ of P_{nn} is accumulated at $R > 1.1\,\mu$m.

To obtain the yield of $(n+2)P$ atoms, the Landau–Zener transition probability is calculated for each state, including sublevels, for all crossings. P_{nn} is also calculated for each n and its sublevels. The $(n+2)P$ atom yield for a specific n, $N_{(n+2)p}$, can then be written as

$$N_{(n+2)p} = \sum_i \frac{P_{\mathrm{react}}^{(i)} P_{nn} N_{\mathrm{gs}}}{16}, \tag{2}$$

where $N_{\mathrm{gs}} = \rho_{\mathrm{gs}} V$ is the number of ground state atoms in the laser excitation volume, V, and the sum is over all the crossings, i, that lead to $(n+2)P$ states. The factor of 1/16 is the excitation probability for a pair of ground state atoms, which we assume to be saturated. Since the process is a near resonant two-photon incoherent excitation, there is a 1/4 probability of excitation for each atom and an overall 1/16 probability for a pair. The results of these calculations are shown in figure 3.

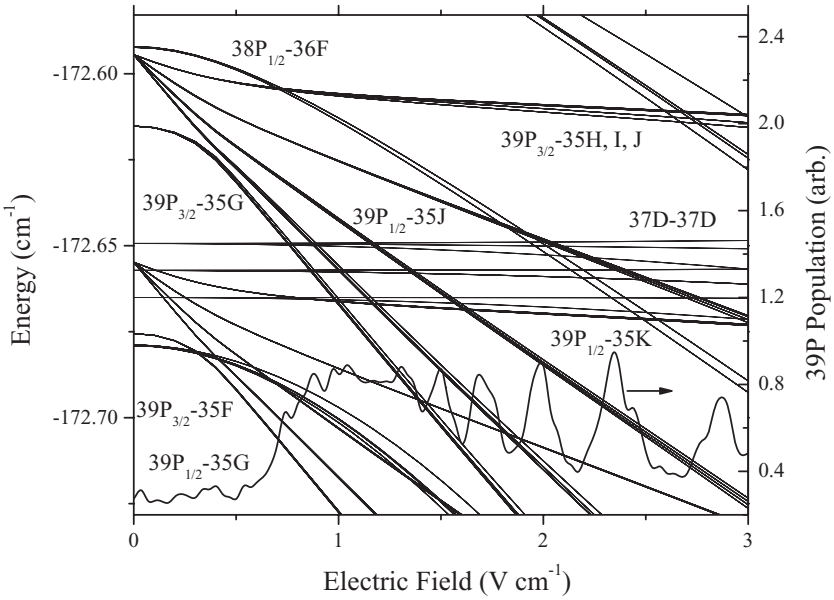

Figure 6. $39P$ atom population and asymptotic atomic pair state energy as a function of ϵ. For simplicity, only states up to $l = J$ are shown. Note that this plot also does not show the interaction of the curves or the sub-states involved.

Note that our experimental results are well explained by the straightforward Landau–Zener model that we used. In contrast, experiments on $nS+nS$ pairs found that ac Stark shifts induced by a laser can lead to atomic population transfer [12]. Here, for the case of $nD+nD$ pairs, where the interaction potentials are attractive, we did not find any significant coupling to nP states due to ac Stark shifts caused by the excitation laser. In [12], the $nS+nS$ states studied were all repulsive. In the case of the $nS+nS$ repulsive states, the nonadiabatic processes were not significant since the small R region where the nonadiabatic transitions occur cannot be reached. It is also important that the energy separation between the $nD+nD$ and $(n+2)P+(n-2)F$ states is much smaller than the energy separation between the $nS+nS$ and $(n+1)P+nP$ states. For the $nD+nD$ pairs, the Stark shifts relative to the $(n+2)P+(n-2)L$ states essential to the present work are much smaller.

4. Discussion

The peak in the decay rates shown in figure 3 for $n = 37$ is the result of $39P+35L$ states being Stark shifted through the $37D+37D$ states, where L labels the states with $l > 2$. These pair states, which have both $39P$ and Stark fan character, shift strongly with electric field. More crossings that lead to $39P$ atom yield appear as ϵ is increased. In figure 6, we show the $39P$ atom population and the asymptotic atomic pair state energy, respectively, as a function of ϵ. Figure 6 also demonstrates that the decay rates can be manipulated by changing ϵ and shows the multi-state nature and complexity of this control. Note that the decay rate can be varied by a factor of $\sim$ 3–5 by changing ϵ from 0.1 to 3.0 V cm^{-1} for $n = 37$. For simplicity, we also show only angular momentum states up to $l = J$. It should also be stated that each peak in figure 6 is the result of many sub-states crossing and we are only plotting the asymptotic energies to show

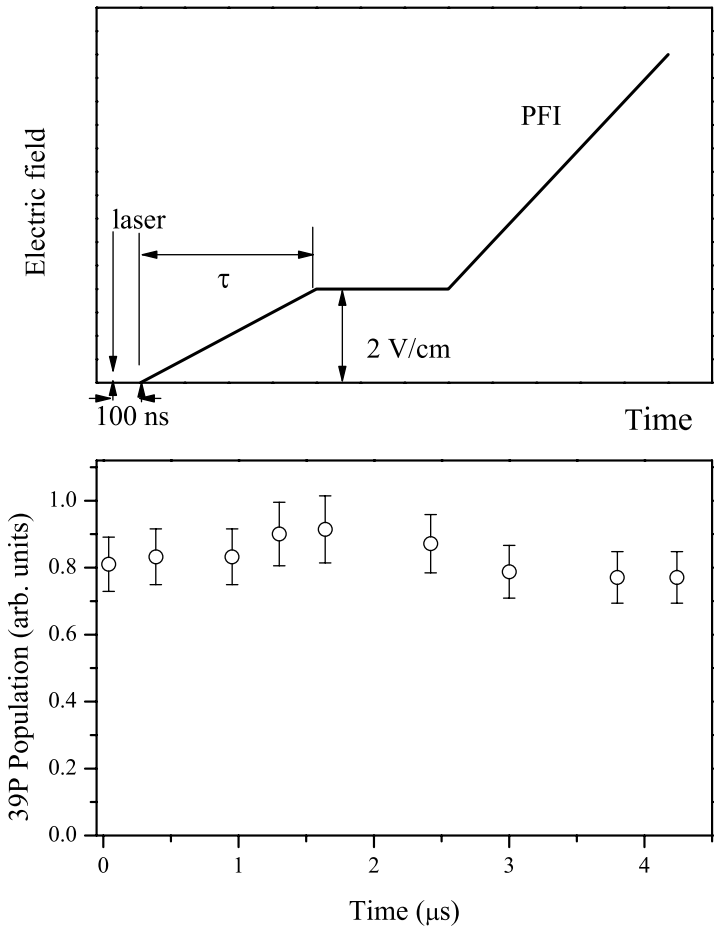

Figure 7. (a) Time sequence for the variable rise time ramp and PFI, where τ is variable. (b) $39P$ population as a function of τ. Clearly the population does not depend on this parameter.

a rough correlation. The actual behavior is much more involved since most of these states are interacting. A full calculation of the theoretical curves for figure 6 requires a calculation like that found in figure 3 for each electric field. This is beyond the scope of this paper.

We point out that the PFI effect observed in [17] could occur in our experiment. However, we believe that it plays a minor role here. In order to verify this we have used the ionization pulse shown in figure 7(a) to ionize atoms in the $39P$ state after the excitation of the $37D$ state. The pulse begins 100 ns after the laser pulse and rises to 2.0 V cm^{-1} in a time, τ, which is varied from 40 ns to 4 μs. The slew rate was varied from 0.5 to 50.0 V μs^{-1}. At 6 μs after the pulsed laser is applied, the electric field rises to a value high enough to ionize the $37D$ state. Figure 7(b) clearly shows that the $39P$ population does not depend on τ.

It is well known that blackbody radiation transfers population to the $(n+2)P$ state, especially at low Δn [13]. In another experiment, we measured the time evolution of the $(n+2)P$ electron signal up to 8 μs after the $nD+nD$ state excitation to determine the blackbody radiation contribution. We used a third boxcar gate to detect the time-dependent population of the states lying energetically above the nD state, N_{up}. Since these upper states can only be excited by blackbody radiation, their populations are a nonadiabatic process free measurement

of the blackbody transfer. We compared these measurements with a rate equation model for blackbody radiation transfer, which considers the induced and spontaneous transition rates involving the following states for each n: (i) from $(n-1)P$ to $(n+4)P$; (ii) from $(n-3)D$ to $(n+3)D$; and (iii) from $(n-4)F$ to $(n+1)F$. Other angular momentum states were not considered in the model because their contribution is small for the timescales studied. Decay to lower states is taken into account by using a single channel. The procedure implemented here is similar to the one used in [18]. All the states above nD will contribute to the population, $N_{\rm up}$, measured with the third boxcar. The measured $(n+2)P$ state population, $N_{(n+2)P}$, will have contributions due to the blackbody radiation transfer and two-body processes. By fitting the theoretical value of $N_{\rm up}$ to the experimental plot, we obtain the blackbody radiation transfer to the $(n+2)P$ state population. The $(n+2)P$ population is subtracted from the experimental measurement. This allows us to obtain the $(n+2)P$ state population without contributions from blackbody radiation transfer. As an example, we show the experimental data and theoretical model in figure 8(a) for $n=29$. Using these calculations, we can eliminate the blackbody contribution to the $(n+2)P$ yield.

The $(n+2)P$ signal due to nonadiabatic transitions grows linearly in time for $t<8\,\mu$s (figure 8(a)). The rate depends on n and ϵ. In figure 8(b), we show the experimental and theoretical $(n+2)P$ signal rates as a function of n for $\epsilon=0.5$ and $2\,{\rm V\,cm^{-1}}$. The theoretical rates shown are obtained by calculating the coupling matrix elements of the Hamiltonian at the curve crossings and using the Golden Rule to obtain the rates. The agreement between the measured and theoretical rates is consistent with our interpretation of the data as decay of a $nD+nD$ quasi-molecule. Nonadiabatic decay is distinct from other Rydberg pair decay mechanisms and is very general because it occurs for almost every attractive pair state at short enough R. Nonadiabatic decay can be added to Penning ionization [19], molecular blackbody decay [20], excitation transfer [21] and many-body effects [22] as an important experimental consideration.

It is valid to interpret the time-dependent experiment as the impulsive excitation of a pair of nD atoms, a nonstationary state, with subsequent time evolution. Because the excitation laser's frequency bandwidth is much larger than the coupling rate to the $(n+2)P$ state, the laser pulse initially excites a wavepacket that has the character of two nD atoms, a so-called 'zeroth' order state (inset of figure 8). The nD atoms carry the oscillator strength for the excitation. As time progresses and the system is able to evolve under the influence of the atom–atom interactions, the $nD+nD$ wavepacket propagates in time and $(n+2)P$ products appear on a timescale inversely proportional to the nonadiabatic transition rate. This is the standard picture for nonadiabatic transitions in the time domain, except that here the timescale is $\sim\mu$s [15]. This point is illustrated for a Landau–Zener crossing shown in figure 9 for the $37D+37D$ state as an example for the cases of, (a) dipole interactions only and (b) both dipole and quadrupole interactions. In figure 9(c), the plots show the $37D+37D$ character and the sum of all $39P+nL$, where $L>2$, for the $37D+37D$ (upper plots) and $39P+35K$ (lower plots) potential curves at $R=1.75\,\mu$m, $R=2.0\,\mu$m and $R=3.0\,\mu$m. We sum the $39P+nL$ character to simplify the figure. The atomic characters are obtained by calculating $|\langle\Psi|nl'n'l''\rangle|^2$, where Ψ is the Rydberg pair wavefunction and $\langle nl'n'l''|$ is the asymptotic two-atom state. There are qualitative differences in the potential energy curves and characters. Interestingly, the state corresponding to the lower curve is affected more because it is interacting strongly with several other states. The changing character of the states as R decreases is the result of the interactions between the atoms. As the virtual transitions between a pair state and its strongly coupled neighboring

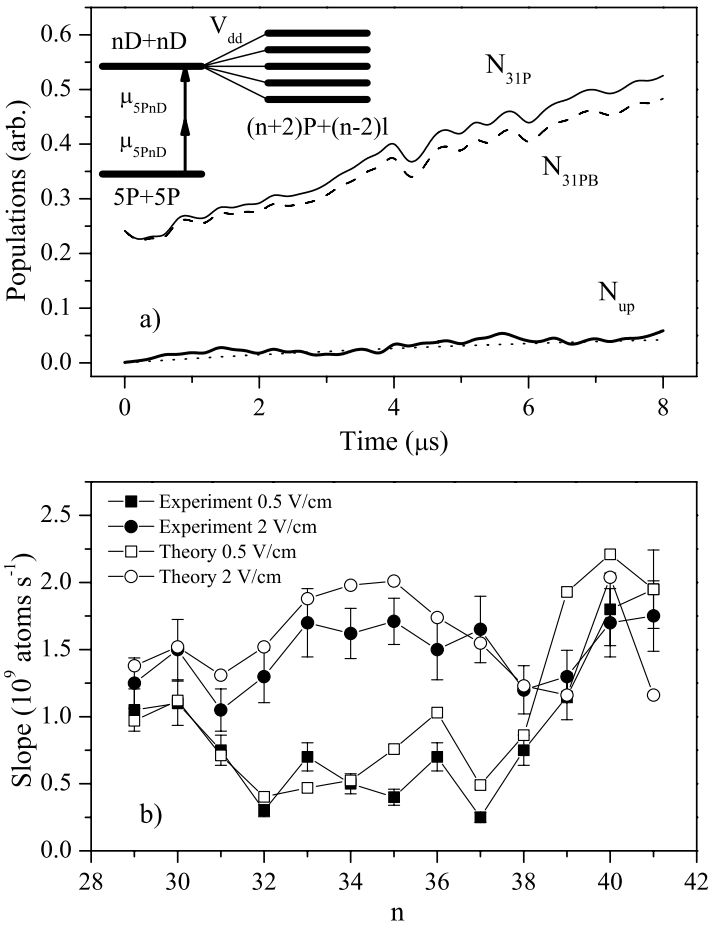

Figure 8. (a) N_{31P}, N_{31PB} and $N_{\rm up}$ populations as a function of time for $\epsilon = 0.5\,{\rm V\,cm^{-1}}$. The dashed line is the blackbody radiation transfer population obtained with the rate equation model. The inset depicts the time-dependent picture. The $nD+nD$ state is a 'bright' dipole allowed state, whereas the $(n+2)P+(n-2)l$ state is a 'dark' dipole forbidden state. The states are coupled by the interaction V_{dd}. (b) Experimental and theoretical slopes of the $(n+2)P$ population as a function of n for $\epsilon = 0.5$ and $2\,{\rm V\,cm^{-1}}$.

states become stronger, more of the character of these atomic states contribute to its electronic wavefunction and the interaction potential changes accordingly, as shown in figure 9.

Our results have interesting implications for an understanding of population transfer in cold Rydberg gases. It is clear that the decay rates can be manipulated with ϵ and possess a strong n dependence. Such dependences are complicated, particularly if there is a combination of low and high electronic orbital angular momentum states involved. States that have strong Stark shifts (high l) can lead to elaborate multilevel character in the pairwise interactions, as demonstrated. However, we have also shown that it is possible to determine with first-principle calculations the behavior of such states and their interactions. These types of calculations can be used to determine the best states to use for a given experiment. Although we used a rather simple model, more sophisticated dynamical models can be implemented when necessary. For example, a quantum multichannel scattering theory could be used to calculate the probabilities

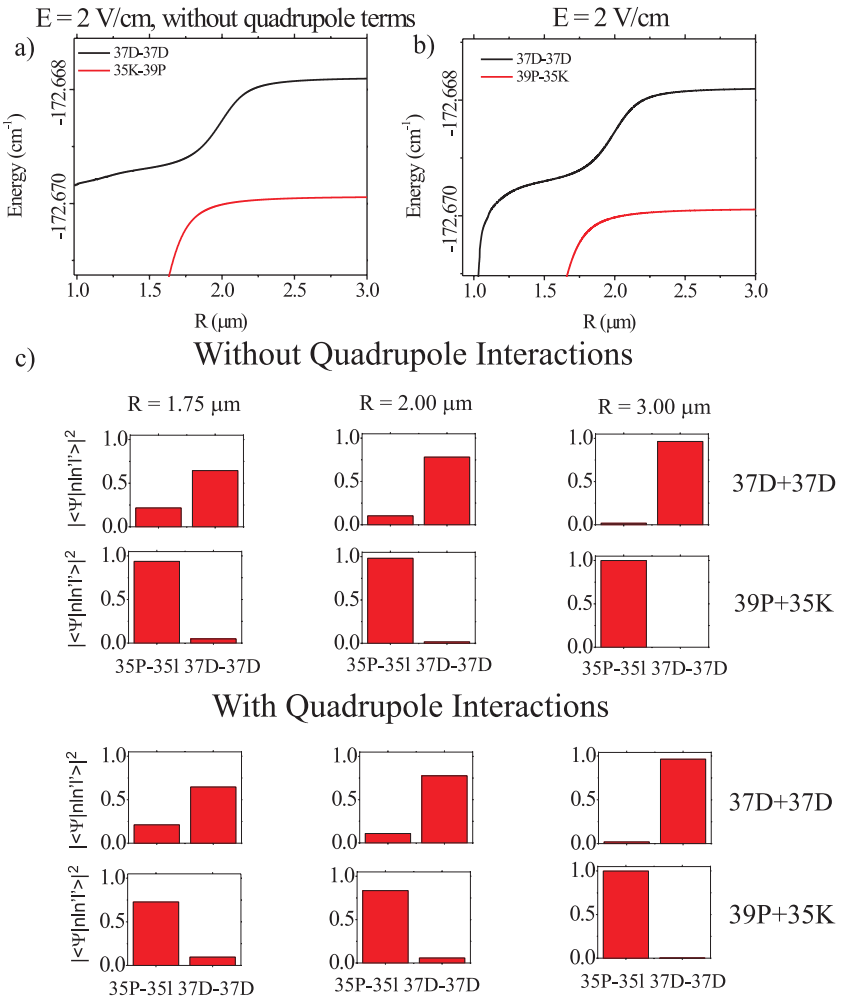

Figure 9. (a) Landau–Zener crossing for $37D + 37D$ and $39P + 35K$ calculated without the quadrupole interaction (dipole interaction only). (b) The same Landau–Zener crossing as in (a), but including the quadrupole interaction and the dipole interactions. (c) Series of plots that show the $37D + 37D$ character and the sum of all $39P + nL$ character, where $L > 2$, at different R. We sum the $39P + nL$ character to simplify the figure. There are qualitative differences in the potential energy curves and characters. Interestingly, the state corresponding to the lower curve is affected more because it is interacting strongly with several other states.

for a pair of Rydberg atoms to change state and a more exact treatment of the excitation process could be applied. In principle, this approach could give more exact rate constants at the cost of a more difficult calculational procedure. We feel a more accurate treatment of the excitation process will lead to the biggest changes. However, the uncertainties in current experiments, such as trap densities, probably limit our ability to distinguish a large difference between our simple model and one that is more exact but complicated.

We also recall that pulsed laser experiments can be interpreted in a time-dependent fashion in ultracold Rydberg gases if the excitation bandwidth is larger than the state-to-state couplings. Q3

To our knowledge, it has not been emphasized that for certain parameters, usually associated with continuous wave excitation, the ultracold Rydberg atom pairs show dynamics more familiar to time-resolved experiments in the ultrafast regime. As far as Rydberg atom blockade is concerned, this point implies that it is advantageous for most applications to use blockade in the limit of time-independent states. However, for experiments on ultracold Rydberg gas dynamics, the time-dependent picture may prove to be more useful, since this way the changing electronic character of the atom pair states with R can be straightforwardly interpreted (figure 9).

5. Conclusion

To summarize, we have studied the role of the dc Stark effect in the decay of $nD+nD$ quasi-molecules. The proposed model, using the Landau–Zener method, was able to reproduce qualitatively and quantitatively the experimental results, suggesting that the multilevel character of the interaction cannot be neglected. In particular, at small R, quadrupolar interactions cannot be ignored. The dc Stark effect may be used to manipulate pair states and their decay rates. We showed that the rate of decay can change by a factor of 3–4 for a modest change in electric field over a large range of n. Pair states with both high and low l components can be particularly sensitive to electric fields and couple strongly to low l pair states. Finally, we have observed a time-dependent effect that suggests that a time-dependent picture may be more appropriate for some ultracold Rydberg atom experiments. This latter point is interesting in its own right because it suggests a way to study the dynamics of cold Rydberg atom interactions and points the way to the study of nonadiabatic molecular dynamics in a regime where measurements can more easily be compared to first-principle calculations, namely μs timescales. Although some of these conclusions are not new, by comparing our experiment to Landau–Zener calculations, we have aimed to clarify some aspects of the pair dynamics that occur in ultracold Rydberg gases.

Acknowledgments

This work was supported by FAPESP, CNPq, INCT-IQ, ARO (W911NF-08-1-0257), NSF (PHY-0855324) and NSF (OISE-0756321). We thank B S Marangoni for technical help.

References

Q4

[1] Jaksch D *et al* 2000 *Phys. Rev. Lett.* **85** 2208
[2] Lukin M D *et al* 2001 *Phys. Rev. Lett.* **87** 037901
[3] Urban E *et al* 2009 *Nat. Phys.* **5** 110
[4] Gaëtan A *et al* 2009 *Nat. Phys.* **5** 115
[5] Younge K C *et al* 2009 *Phys. Rev.* A **79** 043420
[6] Bendkowsky V *et al* 2009 *Nature* **458** 1005
[7] Overstreet K R *et al* 2009 *Nat. Phys.* **5** 581
[8] Farooqi S M *et al* 2003 *Phys. Rev. Lett.* **91** 183002
[9] Schwettmann A *et al* 2006 *Phys. Rev.* A **74** 020701
[10] Schwettmann A *et al* 2007 *J. Mod. Opt.* **54** 2551
[11] Overstreet K R *et al* 2007 *Phys. Rev.* A **76** 011403
[12] Nascimento V A *et al* 2009 *Phys. Rev. Lett.* **102** 213201

[13] Gallagher T F 1994 *Rydberg Atoms* (Cambridge: Cambridge University Press)
[14] Carroll T J *et al* 2004 *Phys. Rev. Lett.* **93** 153001
[15] Schmitt M *et al* 2000 *J. Chem. Phys.* **114** 1206
[16] Chandler D 1987 *Introduction to Modern Statistical Mechanics* (New York: Oxford University Press)
[17] Han J and Gallagher T F 2008 *Phys. Rev.* A **77** 015404
[18] Galvez E J, Lewis J R, Chaudhuri B, Rasweiler J J, Latvakoski H, De Zela F, Massoni E and Castillo H 1995 *Phys. Rev.* A **51** 4010
[19] Amthor T *et al* 2007 *Phys. Rev.* A **76** 054702
[20] Amthor T *et al* 2007 *Phys. Rev. Lett.* **98** 023004
[21] Vogt T *et al* 2006 *Phys. Rev. Lett.* **97** 083003
[22] Younge K C *et al* 2009 *Phys. Rev.* A **79** 043420

QUERY FORM

JOURNAL: NJP

AUTHOR: J S Cabral *et al*

TITLE: Manipulation of quantum state transfer in cold Rydberg atom collisions

ARTICLE ID: njp354812

Page 1

Q1.
Author: Please specify who is the corresponding author and provide his or her email address.

Page 5

Q2.
Author: Please verify the changes made to the sentence 'These assumptions . . . experiments'.

Page 13

Q3.
Author: Please verify the changes made to the sentence ' We also recall that . . . couplings'.

Page 14

Q4.
Author: Please check the details for any journal references that do not have a blue link as they may contain some incorrect information. Pale purple links are used for references to arXiv e-prints.